An Electro-Thermally Actuated Micro-Cantilever-Based Fiber Optic Scanner

Mandeep Kaur, Malcolm Brown, Pierre M. Lane, *Member, IEEE*, and Carlo Menon, *Member, IEEE*

***Abstract*—A sub-millimeter sized optical scanner driven by electro-thermal actuation is presented. The scanner is composed of a single-mode optical fiber (SMF) with a cantilevered section at its distal tip. The fiber cantilever is electro-thermally actuated near its base in a single direction and excited at resonance to obtain large deflections at the tip of the fiber. Two-dimensional imaging of an object is demonstrated by simultaneously rotating the object while scanning across its diameter. Illumination light from the optical core of the fiber cantilever is projected through a lens onto the object. Reflected light is collected by the same lens and projected onto a photodetector. An image of the object is reconstructed by interpolation of the detected signal. The resolution of the system was measured to be 16μm by imaging a resolution target. The electro-thermal fiber actuator may provide a new technique for scanning in sub-millimeter sized forward-viewing endoscopic catheters.**

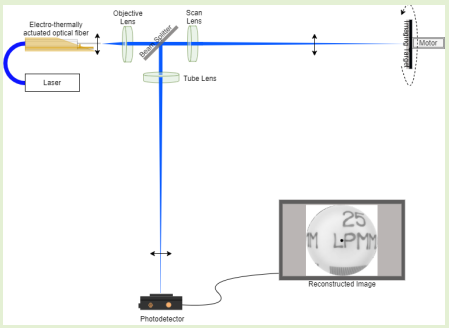

***Index Terms*—Chemical etching, electro-thermal actuator, fiber optic scanner, imaging, mems, micro-cantilever, resonance vibration.**

I. Introduction

OPTICAL scanners provide a means to sweep a small spot of laser light across an object to be imaged. These scanners find use in several applications such as laser printers, barcode readers/scanners, optical switches, 3D printers, laser scanning microscopes, etc. These devices require scanning along one or two directions depending upon the application. Optical fibers provide a compact way to transmit this laser light, permitting the miniaturization of the scanner devices. Fiber optic scanners find frequent use in medical imaging tools such as endoscopes. These minimally invasive instruments assist with diagnostic and therapeutic procedures within internal body cavities and organs.

Manuscript received March 30, 2020; revised April 30, 2020; accepted May 1, 2020. Date of publication May 4, 2020; date of current version August 5, 2020. This work was supported in part by the Natural Sciences and Engineering Research Council (NSERC) of Canada, in part by the Canadian Institutes of Health Research (CIHR), and in part by the Canada Research Chair (CRC) Program. The associate editor coordinating the review of this article and approving it for publication was Dr. Ing. Emiliano Schena. *(Corresponding author: Carlo Menon.)*

Mandeep Kaur is with the MENRVA Research Group, School of Mechatronic System Engineering and Engineering Science, Simon Fraser University, Surrey, BC V3T0A3, Canada.

Malcolm Brown is with the School of Engineering Science, Simon Fraser University, Burnaby, BC V5A1S6, Canada.

Pierre M. Lane is with the BC Cancer Research Center, Imaging Unit, Integrative Oncology, Vancouver, BC V5Z1L3, Canada.

Carlo Menon is with the MENRVA Research Group, School of Mechatronic System Engineering and Engineering Science, Simon Fraser University, Surrey, BC V3T0A3, Canada (e-mail: cmenon@sfu.ca).

Digital Object Identifier 10.1109/JSEN.2020.2992371

The organs that can be imaged by an endoscope are limited by its insertion diameter, so designs must be optimized for a desired imaging area [1]. In conventional endoscopes, the image is captured by a charge-coupled device (CCD) or complementary metal-oxide-semiconductor (CMOS) detectors using reflected light. The smaller the endoscope, the smaller the number of pixel elements in the image sensor. This leads to decreased sensitivity, field of view, lower resolution, and increased sensitivity to noise, especially for endoscopes less than 3mm in diameter [2].

A scanning fiber endoscope (SFE) is characterized by the presence of a single mode optical fiber resonantly actuated at its base, whose inner core delivers light to the surface being imaged. These flexible endoscopes currently allow miniaturization of the distal end to about 1.2 mm. The backscattered light reflected from the tissue surface is collected by outer fibers surrounding the SMF fiber [1]–[5] or by the inner clad of a dual clad fiber. Peak to peak scan amplitude and core diameter of the cantilevered fiber determine the resolution of the image obtained by defining a predetermined number of resolvable points.

Common mechanisms used to actuate the optical fiber include: electrostatic [6], [7], piezoelectric [8]–[17], electromagnetic [18], [19], electro-thermal [20]–[22], micro-motor mirror [23]–[25], and shape memory alloys [26]. Among these, electro-thermal actuators are based on the Joule heating principle, which causes thermal expansion with the passage of current through a resistive medium. Thermal actuation requires more power to substantially excite a fiber than other methods,

but is advantageous in its high magnitude of force, displacement and ease of implementation. Adjusting the frequency of current passing through the actuator, one can easily actuate the cantilever at resonance. Thermal actuators are commonly used in Micro-Electro-Mechanical Systems (MEMS) devices exploiting the U-shaped (bi-morph), V-shaped (Chevron), or Z-shaped configuration [27].

This paper reports the design of a novel, ultrathin, electro-thermally actuated 1D fiber optic scanner vibrating at resonant frequency, which can be packaged within a $\sim 500\mu$m diameter housing. The proposed scanner provides the potential for a sub-millimeter sized forward-viewing endoscopic catheter which is small enough to access the submillimeter sized airways of the lung, pancreatic duct, and fallopian tubes for early cancer screening.

We demonstrate 2D imaging using our 1D fiber scanner by scanning a laser spot over a rotating object and interpolating the reflected light to reconstruct an image. The light emitted from the core of the fiber cantilever is projected on to the object to be imaged and the light reflected by the object is captured by a silicon photodetector. It is a natural extension of the work presented here to rotate the scanner assembly within a small stationary tube instead of rotating the object itself to realize a fully 2-D scanning fiber endoscope.

The manuscript is organized as follows: Section II describes the techniques for fabricating the metallic actuator and the optical cantilever, and the packaging of the sample. The sample characterization for imaging the target using the reflected light is illustrated in Section III. The experimental results are discussed in Section IV altogether with the comparison of the proposed scanner with the available scanners to the date. In the end, the conclusions are presented in Section V.

II. Cantilever Fabrication

The design of the micro-cantilever, electro-thermally excited near its base using a metallic actuator, follows the works described previously in [28]. Briefly, the actuator is made of a thin metallic brass foil with a bridge-like structure, shown in Figure 1, where the periodic current passage causes thermal expansion and contraction of the actuator near the base of the cylindrical cantilever.

In this work, the fiber cantilever is fabricated monolithically by etching the distal 2 mm of a single segment of SMF to reduce it diameter from 125μm down to 12μm. The dimensions of the cantilevered section are selected to get the target scan frequency of 2.5 kHz [28]. Previously, we fabricated the cantilever from a second segment of a multimode fiber, drawn down to 12μm, which was then fusion spliced on to the first segment of SMF [28]. Here we start with a single segment of fiber (460HP, Thorlabs) with a core diameter of 2.5μm.

Matching the frequency of the periodic current to the resonant frequency of the cantilever, one can get higher displacement of the micro-cantilever tip at a given base excitation. To avoid damping, the SMF optical fiber is fixed within a sub-millimeter sized needle prior to the micro-cantilever portion with the help of polymeric collar structures. The schematic design of the proposed setup is shown in Figure 2, which highlights the placement of the cantilevered fiber within the hypodermic needle with respect to the actuator.

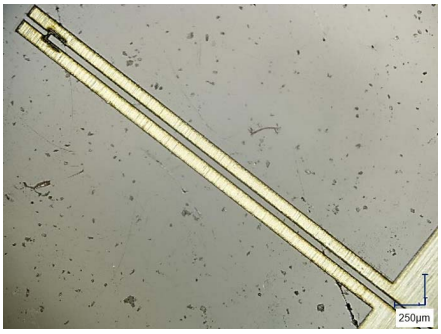

Fig. 1. The laser cutout of the metallic actuator (scale bar = 250μm).

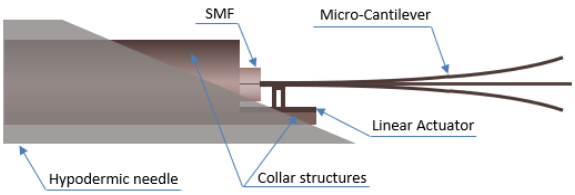

Fig. 2. The schematic design of the packaged assembly.

A. Etching

Chemical etching using hydrofluoric acid (HF) is commonly used to etch the optical fibers to obtain nanometer sized fiber tips used for optical sensors [29]–[31]. Since HF is very dangerous to work with, a buffer solution with stabilized HF activity (Buffer Oxide Etchant or BOE, Transene) is used for etching. BOE solution contains ammonium fluoride (NH_4F) and HF in a standard ratio of 6:1.

In the case of chemical etching, usually there is a formation of a tapered region in the transition zone of the fiber ($\sim 600\mu$m) where it's diameter changes from the original value to the smaller value (from 125μm to about 12μm in our case). This tapered region is present due to the capillary (meniscus) effect which causes a slight raise of the HF solution in correspondence of the surface of the liquid. The raised etching solution along the sidewalls of the fiber reduces its diameter causing the tapered section [32]. In order to avoid the formation of this tapered region to get a cylindrically shaped cantilevered section, the open surface of HF solution should be avoided at all the times during etching. Thus, a thin membrane made up of Ecoflex rubber (Ecoflex 00-20, smooth-on) is attached to a small plastic tray which can float on the surface of HF. Small holes are drilled in the tray and the flexible membrane. The plastic protective sheath on the fibers is stripped away, leaving its diameter to be 125μm, and these are passed through the holes with a protruding length of about 2mm in HF solution. The flexible membrane tends to close the hole around the sidewalls of the fiber during the etching process blocking the raise of solution along the walls and thus avoiding the tapered region. Figure 3 shows the schematic of the setup used for etching process. The BOE solution is contained in a plastic container, on the surface of which a plastic tray floats carrying the fibers. This setup is placed inside a container carrying water on top of a hot plate

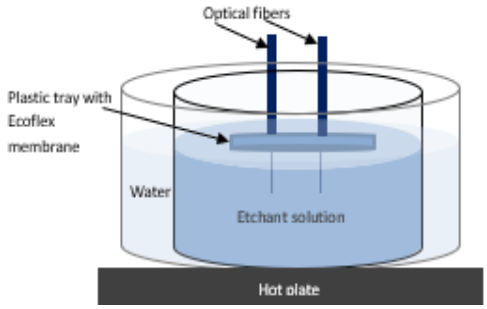

Fig. 3. The schematic of the setup used for etching the optical fibers.

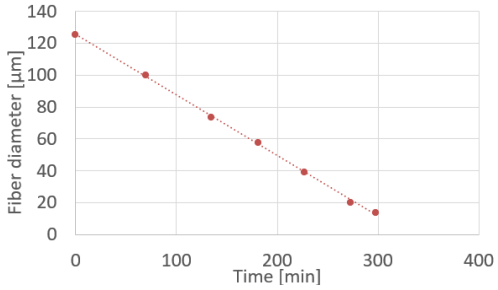

Fig. 4. Fiber diameter as a function of etching time.

Fig. 5. The cantilevered fiber obtained via etching process (scale bar = 250μm).

guaranteeing the uniform temperature of the solution during the etching process.

The etching process is performed by setting the temperature of hotplate at 30°C. Thus, water and the BOE solution is heated up and maintained at constant temperature via hotplate, and the water temperature is measured using a thermometer. After few minutes, a fiber is removed from the solution and monitored under the microscope to characterize its diameter. The diameter reduction of the fiber in time is shown in Figure 4. The diameter of the SMF reduces linearly from 125μm to about 12μm in time with the etching rate of 0.38μm/min, as from the trend line in the figure. The cantilevered fiber obtained with this process is shown in Figure 5.

B. Packaging

The metallic actuator is made up of 25μm thin brass foil affixed to the cantilevered fiber with the help of acrylic (PMMA) collars as described in [28]. The complete packaging process consists of lifting the bridge pattern, placing the SU-8 collar structures on the flat base of the actuator, and the 125μm section of the optical fiber nearby the transient region of the geometry of fiber, attaching the two parts together using thin layer of epoxy (5 minute epoxy, Devcon), applying a

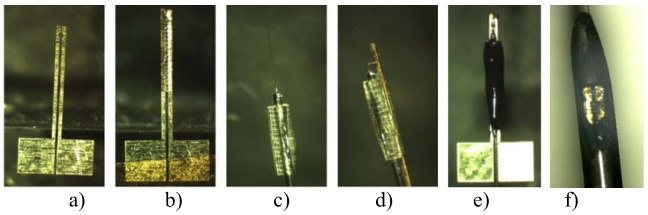

Fig. 6. Packaging of the sample. a) actuator flipped on PDMS structure; b) semi-circle pieces placed in the groove of actuator; c) semi-circle structures placed on SMF fiber; d) side view of assembly; e) assembled device with heat cured epoxy; f) top view of packed device inside the nitinol needle.

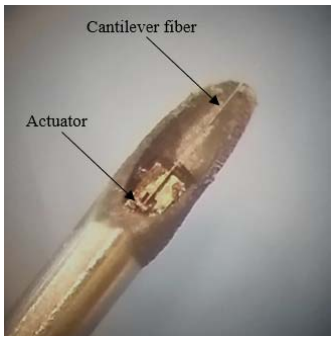

Fig. 7. Packaged scanner sample.

generous amount of heat cure epoxy (EP-17 HTND-CCM, MasterBond), and curing the sample for 6 hours at 170°C. The packaging process has been reported previously [28] and is summarized in Figure 6.

A cured and packaged sample inside the 500μm diameter nitinol needle is shown in Figure 7. The front of the needle is cut down at an angle to monitor the assembled setup under the microscope.

III. Characterization and Imaging

The micro-cantilever is linearly actuated near its base by the metallic bridge. By matching the frequency of the current passing through the bridge to the resonant frequency of the micro-cantilever, a greater tip displacement is obtained. The first resonant (natural) frequency of a cantilever beam with a round cross section is given by:

$$F = \frac{(1.875)^{1/2}}{2\pi}\sqrt{\frac{EI}{\rho AL^4}} = 1.194^2\frac{\pi\sqrt{E}}{16\sqrt{\rho}}\frac{R}{L^2} \qquad (1)$$

where ρ, E, L and R are the density, Young's modulus, length and radius of the cantilever, respectively [33].

The natural frequency as function of these parameters is plotted in Figure 8. Each line in the Figure corresponds to a given length of the cantilever indicated on each line in μm.

As each sample is manually fabricated, there are variations among them, including: position of the bridge along the micro-cantilever's length, epoxy amount, curing time/procedure, fiber dimensions, fiber alignment accuracy with respect to the bridge, etc. Therefore, each sample's resonant frequency is different and is obtained by testing frequencies around ±500Hz of the expected value, and measuring for maximum cantilever tip displacement.

From the length and diameter of the cantilevered fiber measured under the microscope, the theoretical resonant frequency

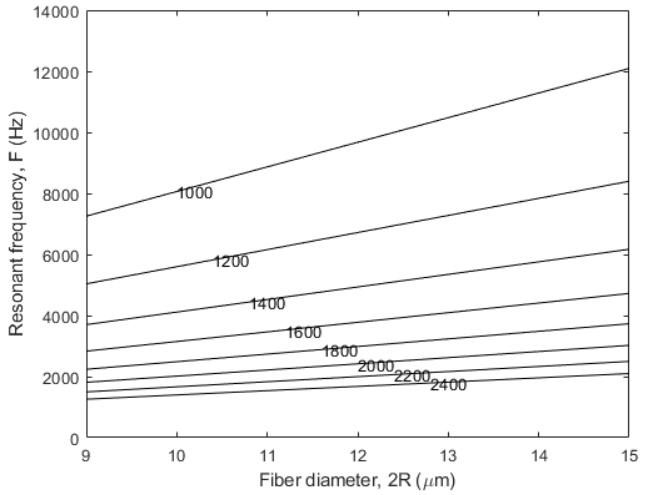

Fig. 8. Resonant frequency in function of the cantilever diameter (2R) and length (L).

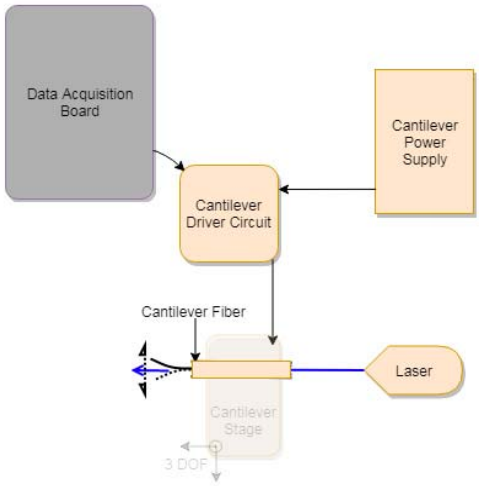

Fig. 9. Schematic diagram of the experimental setup.

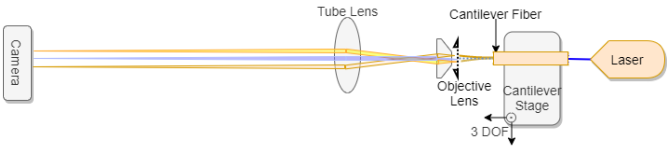

Fig. 10. A conventional diagram of the optical setup used for imaging tip displacement.

is calculated, which is considered as the starting test value for the resonant frequency. The exact resonant frequency is obtained by sweeping the frequency nearby the theoretical value and measuring the amplitude of tip displacement until it reaches the maximum value.

A. Cantilever Drive

The actuator is driven with a square wave in order to obtain a periodic expansion and contraction of the bridge with corresponding excitation near the cantilever fiber base. The duty cycle of the square wave is an important parameter that influences the performance of the sample. At the beginning of a test, a duty cycle of 50% is used to quickly determine the resonant frequency. By decreasing the duty cycle from 50% to 25%, the amplitude of the tip displacement increases (more than double) for a given amount of average power passed through the bridge. After various attempts of different duty cycles, a smaller duty cycle of 6% is used as a standard value for the further tests. Thus, the current is passed through the sample for 6% of the period related to the resonant frequency, and 94% of the time is left without current to allow the heat dissipation from the thin actuator. This also permits the usage of higher current within the sample without damaging it. Thus, it is possible to excite the actuator using a 25V peak-to-peak pulse train, with 0.44A current passing through it. It is possible to drive the samples with even smaller duty cycles, but the required excitation voltage is much higher for desired tip displacement, which can be unsafe for the actuator itself given its small dimensions.

A schematic diagram of the test setup is depicted in Figure 9. The data acquisition (DAQ) board sends a square wave signal to the driver circuit, which is powered by an external DC supply. The output of the circuit is connected to the metal foil conduction wires which are non-polar.

B. Scan Characterization

A schematic of the optical setup used to characterize the in-plane scan pattern is shown in Figure 10. The sample is mounted on a three degrees of freedom (DOF) stage, allowing its alignment with the optical lenses. A 450 nm blue laser (LP450-SF15, Thorlabs) is connected to the input pigtail of the of the fiber cantilever. The scan pattern is projected on to a CMOS camera (STC-MBE132U3V, Sentec) by an objective lens (f=16.5mm) and tube lens (f=300mm) as shown in the figure.

The in-plane scan pattern imaged by the CMOS camera is shown in Figure 11a. The image was generated by setting the bridge current at the cantilever's natural frequency with a 6% duty cycle. Overall tip displacement is about 213μm in the direction of base excitation.

A brass sample attached to a glass slide with a 150μm long bridge was monitored under a microscope (VHX-2000, Keyence) and is shown in Figure 11b. From the side view image, the cantilever fiber appears to oscillate in a linear manner. However, the tip displacement may be non-linear due to reasons such as: asymmetry of the bridge and/or cantilevered fiber, pretension in the cantilever, etc. These deviations from the ideal can generate a whirling motion in the fiber, i.e. the path of light is elliptical instead of a line [34]–[36].

The cantilevered fiber in our case is characterized by having a circular surface which leads to fact that the ratio of natural frequencies in two principal planes is one. Thus, the plane motion becomes unstable, and follows an elliptical shape pattern at steady state in a plane normal to the cantilever axis. The equations of motion characterizing this elliptical shape pattern of the whirling motion are described in detail in [34]. The elliptical motion can be modified to be more linear by changing the driving frequency to be slightly off from the natural frequency, but the fiber would not be operating at resonance causing a smaller tip displacement.

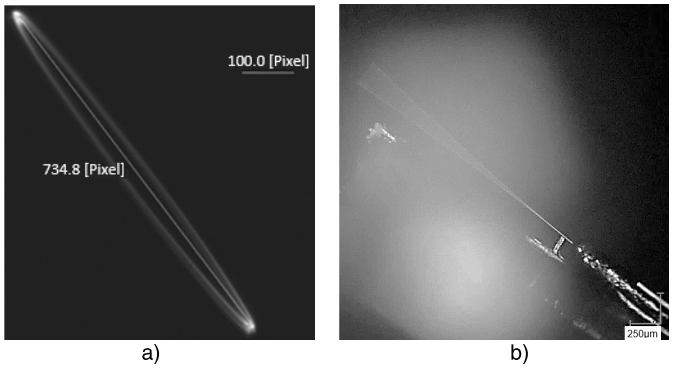

Fig. 11. Tip displacement of the cantilever under actuation. a) front view; b) side view.

C. Imaging Setup

Light from the fiber cantilever is projected on to the object to be imaged by an objective lens (f=16.5mm) and scan lens (f=150mm) as shown in Figure 12. Back reflected light from the object is collected by the scan lens and refocused by a tube lens (f=150mm) on a photo detector (PDA100A2, Thorlabs).

Light from the fiber is collimated as it passes through the objective lens. Half the light is focused on the object by the scan lens after passing through a 50/50 beam splitter. The light reflected from the object passes back through the scan lens and is projected on the photo detector. The output of the detector is connected to a DAQ board (USB X Series 6341, National Instruments). The DAQ board collects the analog intensity data from the photodetector to be processed into the scanned image.

D. Image Acquisition

A polar scanning geometry is used to create a two-dimensional image. The cantilever scans across the object to be imaged (fast axis of the scan) while the object rotates (slow axis of the scan). The frequency of rotation can be increased for higher frame rate or decreased for better resolution. For example, a fiber with a diameter of 12μm and length of about 2mm (having a resonant frequency of 2.5 kHz) at 30 frames per second will have ~166 fast-axis scans per frame. At half the frame rate twice as many fast-axis scans occur.

A schematic diagram of the imaging setup is shown in Figure 12. A variable frequency resolution target (Variable Frequency Target 5-200 lp/mm, Edmund Optics) is used as the object to be imaged. The resolution target is attached to the shaft of a stepper motor using a 3D-printed holder. The motor carrying the resolution target is mounted on a three degrees-of-freedom stage, allowing the alignment of the center of the rotating target with the incoming light beam.

The DAQ board was programmed to provide the timing signals for the system. The same computer program also interpolated the sampled data and displayed images in real time. The cantilever resonant frequency, duty cycle, cantilever tip phase offset, number of samples per line, and the number of lines per rotation were configured through the program. The DAQmx board generated the timing signals required for the cantilever drive circuit and the motor. Rotation of the motor is synchronized with the cantilever. The light intensity is sampled

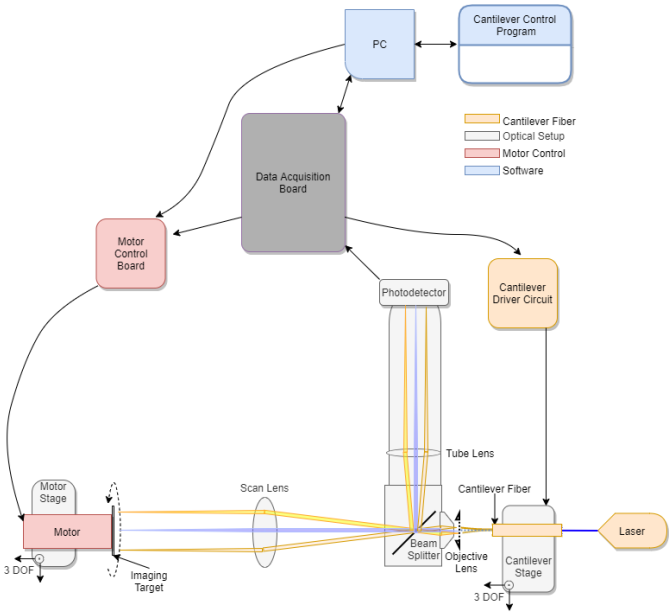

Fig. 12. Schematic diagram of the complete testing setup.

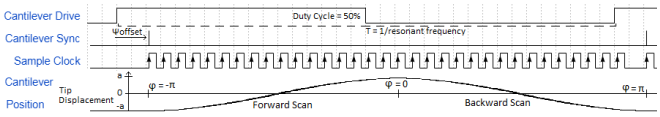

Fig. 13. Timing diagram for image acquisition.

by an analog-to-digital convertor. The line timing is illustrated in Figure 13.

The Cantilever Drive signal is generated by the DAQmx board using the resonant frequency of the cantilever and a desired duty cycle. Digitization of scanline intensity is triggered by the Cantilever Sync signal which is delayed in time from the rising edge of Cantilever Drive to account for the phase shift ($\boldsymbol{\Psi_{offset}}$) between the drive waveform and the actual cantilever tip position. The scanline intensity is sampled by the Sample Clock signal.

E. Interpolation

We assume the cantilever tip follows a sinusoidal pattern in time so that the tip displacement in spatial coordinates $(\boldsymbol{x}, \boldsymbol{y})$ can be modeled as an ellipse with major axis $\boldsymbol{2a}$ and minor axis $\boldsymbol{2b}$. As illustrated in Figure 14, the cantilever tip traces out one complete elliptical cycle as $-\boldsymbol{\pi} < \boldsymbol{\varphi} < \boldsymbol{\pi}$.

Consequently, the tip position $(\boldsymbol{x}, \boldsymbol{y})$ of a cantilever rotated through an angle $\boldsymbol{\theta}$ can be represented as the product of a rotation matrix and a position matrix parameterized by $\boldsymbol{\varphi}$,

$$\begin{bmatrix} x \\ y \end{bmatrix} = \begin{bmatrix} \cos\theta & -\sin\theta \\ \sin\theta & \cos\theta \end{bmatrix} \begin{bmatrix} a\cos\varphi \\ b\sin\varphi \end{bmatrix} \quad \begin{matrix} -\pi < \varphi < \pi \\ -\pi < \theta < \pi \end{matrix} \tag{2}$$

Equation 2 can therefore be used to describe cantilever tip position $(\boldsymbol{x}, \boldsymbol{y})$ as the cantilever scans (elliptically) in the radial direction $(-\boldsymbol{\pi} < \boldsymbol{\varphi} < \boldsymbol{\pi})$ and the object being imaged (or the scanner assembly) rotates in the azimuthal direction $(-\boldsymbol{\pi} < \boldsymbol{\theta} < \boldsymbol{\pi})$.

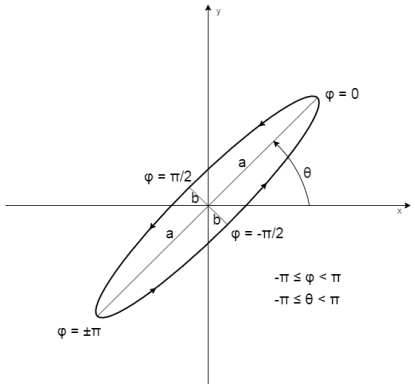

Fig. 14. Rotating ellipse representing the cantilever's tip displacement.

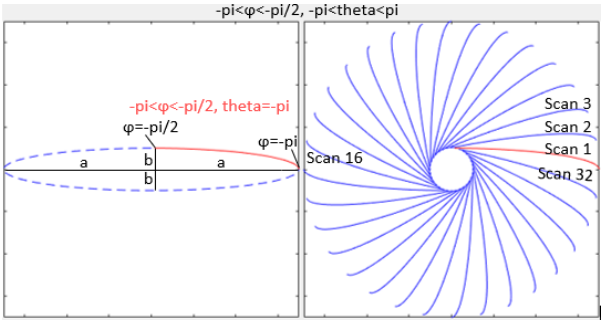

Fig. 15. Quarter of ellipse traced in time.

The image intensity is sampled uniformly in $(\boldsymbol{\varphi}, \boldsymbol{\theta})$ space and must be interpolated for uniform sampling in $(\boldsymbol{x}, \boldsymbol{y})$ space. In general, inverting Equation 2 and solving for $(\boldsymbol{\varphi}, \boldsymbol{\theta})$ in terms of $(\boldsymbol{x}, \boldsymbol{y})$ provides 4 solutions. One solution is,

$$\theta = \arctan \frac{bx\sqrt{a^2 - r^2} - ay\sqrt{b^2 + r^2}}{-by\sqrt{a^2 - r^2} - ax\sqrt{b^2 + r^2}}$$
$$\varphi = \arctan \sqrt{\frac{-a^2 - r^2}{b^2 - r^2}} \tag{3}$$

where we have defined $\boldsymbol{r}^2 = \boldsymbol{x}^2 + \boldsymbol{y}^2$. This solution corresponds to a radial forward scan and includes sample points such that $-\boldsymbol{\pi} \leq \boldsymbol{\varphi} < -\frac{\boldsymbol{\pi}}{\boldsymbol{2}}$ and $-\boldsymbol{\pi} < \boldsymbol{\theta} < \boldsymbol{\pi}$, illustrated in Figure 15 by the red arm of the ellipse. The other three solutions correspond to the other half of the forward scan and the backward scan. When the cantilever scan is linear $(\boldsymbol{b} = \boldsymbol{0})$, Equation 3 simplifies to $\boldsymbol{\theta} = \mathbf{tan}^{-1}\frac{\boldsymbol{y}}{\boldsymbol{x}}$ and $\boldsymbol{\varphi} = \mathbf{cos}^{-1}\frac{\boldsymbol{r}}{\boldsymbol{a}}$.

An **M**-by-**N** pixel interpolation table is constructed, where $\boldsymbol{m} = \mathbf{0}, \mathbf{1}, \ldots \boldsymbol{M}-\mathbf{1}$, $\boldsymbol{n} = \mathbf{0}, \mathbf{1}, \ldots \boldsymbol{N}-\mathbf{1}$, **M** is the width of the image, and **N** is the height. Discrete pixel $(\boldsymbol{m}, \boldsymbol{n})$ is related to continuous position $(\boldsymbol{x}, \boldsymbol{y})$ using,

$$x = a(\frac{2m}{M} - 1) \quad y = a(\frac{2n}{N} - 1) \tag{4}$$

The $(\boldsymbol{\varphi}, \boldsymbol{\theta})$ elements for the interpolation table are then calculated using Equations 3 and 4.

The resolution target is shown in Figure 16. An image of the resolution target acquired with the cantilever fiber placed perpendicularly to the brass foil bridge is shown in Figures 17, and 18. As discussed earlier, the cantilever tip traces an elliptical scan and the 2D scan is obtained by rotating such

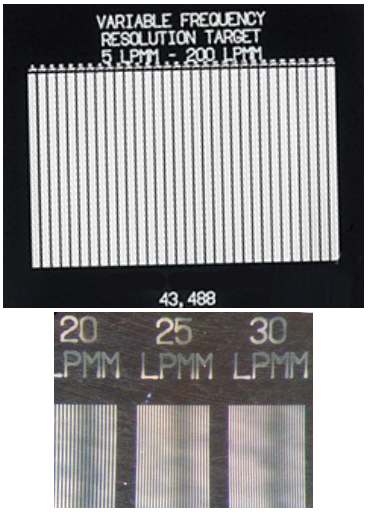

Fig. 16. Resolution target used as imaging object.

Fig. 17. Reconstructed image of the resolution target corresponding to 25lp/mm.

elliptical pattern, which leads to no image data being available in its center (within a circle of radius b, seen as a black circle in Figure 17, eg.). The imaged section of the resolution target shown in Figure 17 corresponds to a 25lp/mm area. Figure 18 shows the lines pattern and the numbers written in the nearby space corresponding to 30lp/mm features. This means that the smallest resolvable line feature has a width of 16.67μm. Due to the higher density of data points near the center, the image is much sharper in that area.

IV. Discussion

The experimental results show the promising performance of the proposed optical scanner. The peak tip displacement of the cantilevered fiber increases linearly with the current supplied to the actuator and shows an elliptical shaped pattern due to the whirling effect at higher power. The ellipticity and the voltage at which it becomes prominent depends highly on the sample. Some samples show the ellipse pattern at about 10V while others can have a near-linear pattern even at 22V. The ellipticity can be reduced by offsetting the actuation frequency from resonant frequency, or lowering power, but the overall displacement of the scanning fiber will decrease as well. Duty cycle also affects the performance of the sample. A smaller duty cycle allows more time for heat dissipation.

Fig. 18. Acquired image of the resolution target at 30lp/mm.

For a given average power, it means that more power can be used in the shorter on phase, causing greater tip displacement. However, the high peak temperature reached with small duty cycles can lead to damage to the bridge and the sample itself. 6% duty cycle is used for testing the samples as it permits the desired tip displacement without damaging the sample.

There are some variations among the samples during its fabrication process. As stated earlier, these differences cause the resonant frequency and performance of the sample to be different. The fabrication process can be optimized to produce the similar sample. Etching permits the batch fabrication of the cantilevered fibers. Thus, similar fibers can be generated by etching a large number of fibers at the same time. Moreover, the fiber position with respect to the actuator can be controlled by using step shoulders.

Current samples are mounted on glass slides for ease of handling, which limits direct rotation to get 2D images from 1D actuation. In future samples, the glass slide will be omitted. This will permit rotation of the cantilevered assembly instead of the image target. In that case, the current scanner can be potentially used as endoscopic catheter having sub-millimeter dimensions. The image obtained from the device is highly affected by optical parts used for imaging. For endoscopic purposes, the currently used lens system will be replaced by a much smaller grin lens. The optical fiber itself will then be replaced by a double clad fiber (DCF) where reflected light will be captured by its inner cladding. The reflected light signal will be separated from the core signal using a Double Clad Fiber Coupler (DCFC) before reaching the detector for processing.

The elliptical shape of the fiber tip's motion means there is no data available of the central image area. This area can be reduced by exciting the fiber at lower frequencies. The reconstructed images show a small distortion at the bottom. The reconstruction algorithm can be slightly updated by recalibrating it to avoid such distortions, and make the images more clear and sharp.

Smaller endoscopes will enable the visualization the peripheral airways, fallopian tubes, and other small luminal organs that are currently inaccessible to conventional endoscopy. Currently, the smallest scanning fiber endoscope has an outer diameter of almost 1.2mm [1]. The main factors limiting further miniaturization are the actuation method (piezoelectric actuator in [1]) and collection fibers size. These limitations are overcome using an electro-thermal actuator (small sized actuators produce large forces) and by collecting reflected light with the inner cladding of the DCF fiber. The proposed catheter can be assembled within a 500μm hypodermic needle. Experimental results validate the proposed model and the optical setup shows the image of the reflecting surface with a resolution of about 16.67μm. The world's smallest image sensor (OV6948, OmniVision) has the size of 575μm x 575μm, and can process video with the frame rate of 30fps [37]. Thus, it is possible to process the video at the rate comparable to OV6948 camera within the even smaller device size. On the other side, the image area is slightly small in the proposed catheter (200μm across compared to 364μm across). Some properties of the proposed optical scanner are summarized and compared with the current MEMS in Table I.

TABLE I
COMPARISON OF DIFFERENT AVAILABLE MEMS SCANNERS WITH THE PROPOSED SAMPLE

	Working principle	*Frequency*	*Scanned area*	*Power consumption*	*Scanner dimensions*	*Scanning pattern*
Electrothermal MEMS fiber scanner [21,38]	Electrothermal actuation	239Hz (x-axis) 207Hz (y-axis)	378µm x 439µm	16Vpp (duty cycle - 13%)	Diameter (1.65mm) Length (28mm)	Lissajous scanning
Lissajous fiber scanner [39]	Piezoelectric tube	86Hz (x-axis) 97Hz (y-axis)	732µm x 591.7µm	40Vac	Diameter (3.2mm) Length (50mm)	Lissajous scanning
OCT based on 2D MEMS mirror [23]	Electrothermal actuation	1.25Hz (fast scan actuator pair) 0.0125Hz (longitudinal)	2.3mm x 2.3mm	0-4V ramp (fast scan) 0.5-3.5V ramp (slow axis)	Diameter (5.8mm) Length (12mm)	Lissajous scanning
OCT probe based on a tilted MEMS mirror [24]	Electrothermal bimorph actuators	750Hz	2.2mm x 2.2mm	5Vdc	Diameter (2.7mm) Length (40mm)	Raster scanning
Scanning fiber endoscope [1]-[5],[40,41]	Piezoelectric tube	5kHz	200µm (in diameter)	<20Vac	Diameter (1.2mm - 1.7mm) Length (9mm)	Spiral scan pattern
Bimodal endoscopic imager [14]	Piezoelectric tube	715Hz	1.17mm (in diameter)	61mW	Length (15mm) width (2.4mm) height (3.3mm)	Spiral scanning pattern
Multi-Photon Endoscope [16]	Piezoelectric tube	35Hz	900µm (in diameter)	40Vac	Diameter (5mm) Length (4cm)	Circular pattern
OmniVision camera [37]	Chip on tip camera	-	364µm x 364µm	3.3Vac	650µm x 650µm x 1158µm	-
Proposed optical scanner	Electrothermal actuation	~2.5kHz	213µm (in diameter)	21Vpp (duty cycle - 6%)	~500µm diameter Length(<7 mm)	Propeller pattern

V. Conclusions

An optical scanner actuated in one direction using an electro-thermal actuator is presented. The thermal expansion of the metallic surfaces of the actuator excites the cantilevered optical fiber to sweep a laser across a sample. Matching the frequency of the current supplied to the actuator, the cantilever is vibrated in resonance to get higher tip displacement. The vibrating fiber projects light along a linear/elliptical path on the object to be scanned. By rotating the target, the 1D scanner is used to demonstrate scanning of a 2D pattern. The device may provide a new means for scanning in sub-millimeter sized endoscopic catheters with dimensions smaller than the current smallest camera, and at similar frame rate.

References

[1] C. M. Lee, C. J. Engelbrecht, T. D. Soper, F. Helmchen, and E. J. Seibel, "Scanning fiber endoscopy with highly flexible, 1 mm catheterscopes for wide-field, full-color imaging," *J. Biophoton.*, vol. 3, nos. 5–6, pp. 385–407, 2010.

[2] E. J. Seibel, Q. Y. J. Smithwick, C. M. Brown, and P. G. Reinhall, "Single-fiber flexible endoscope: General design for small size, high resolution, and wide field of view," *Proc. SPIE*, vol. 4158, pp. 29–39, Jan. 2001.

[3] P. G. Reinhall, "Optomechanical design and fabrication of resonant microscanners for a scanning fiber endoscope," *Opt. Eng.*, vol. 45, no. 4, Apr. 2006, Art. no. 043001.

[4] E. J. Seibel, R. S. Johnston, and C. D. Melville, "A full-color scanning fiber endoscope," *Proc. SPIE*, vol. 6083, Feb. 2006, Art. no. 608303.

[5] E. S. Barhoum, R. S. Johnston, and E. J. Seibel, "Optical modeling of an ultrathin scanning fiber endoscope, a preliminary study of confocal versus non-confocal detection," *Opt. Express*, vol. 13, no. 19, pp. 7548–7562, 2005.

[6] J. M. Zara, S. Yazdanfar, K. D. Rao, J. A. Izatt, and S. W. Smith, "Electrostatic micromachine scanning mirror for optical coherence tomography," *Opt. Lett.*, vol. 28, no. 8, pp. 628–630, Apr. 2003.

[7] A. D. Aguirre *et al.*, "Two-axis MEMS scanning catheter for ultrahigh resolution three-dimensional and en face imaging," *Opt. Express*, vol. 15, no. 5, pp. 2445–2453, 2007.

[8] X. Liu, M. J. Cobb, Y. Chen, M. B. Kimmey, and X. Li, "Rapid-scanning forward-imaging miniature endoscope for real-time optical coherence tomography," *Opt. Lett.*, vol. 29, no. 15, pp. 1763–1765, Aug. 2004.

[9] H.-C. Park, Y.-H. Seo, K. Hwang, J.-K. Lim, S. Z. Yoon, and K.-H. Jeong, "Micromachined tethered silicon oscillator for an endomicroscopic lissajous fiber scanner," *Opt. Lett.*, vol. 39, no. 23, pp. 6675–6678, Dec. 2014.

[10] G. Huang and Z. Ding, "Rapid two-dimensional transversal scanning fiber probe for optical coherence tomography," *Proc. SPIE*, vol. 6429, Feb. 2007, Art. no. 64292W.

[11] Z. Liu, L. Fu, F. Gao, and X. Zhang, "Design and implementation of a 2-D endoscopic optical fiber scanner," *Proc. SPIE*, vol. 7280, Mar. 2009, Art. no. 72801D.

[12] T. Wu, Z. Ding, K. Wang, M. Chen, and C. Wang, "Two-dimensional scanning realized by an asymmetry fiber cantilever driven by single piezo bender actuator for optical coherence tomography," *Opt. Express*, vol. 17, no. 16, pp. 13819–13829, Aug. 2009.

[13] G. Li, H. Gao, A. Zhou, and Z. Liu, "Endoscope two dimensional scanning fiber probe and the driving method," *Proc. SPIE*, vol. 8199, Nov. 2011, Art. no. 819913.

[14] S. Kretschmer, J. Jäger, S. Vilches, Ç. Ataman, and H. Zappe, "A bimodal endoscopic imager in a glass package," *J. Micromech. Microeng.*, vol. 28, no. 10, Oct. 2018, Art. no. 105009.

[15] A. Rajiv, Y. Zhou, J. Ridge, P. G. Reinhall, and E. J. Seibel, "Electromechanical model-based design and testing of fiber scanners for endoscopy," *J. Med. Devices*, vol. 12, no. 4, 2018, Art. no. 041003.

[16] F. Akhoundi, Y. Qin, N. Peyghambarian, J. K. Barton, and K. Kieu, "Compact fiber-based multi-photon endoscope working at 1700 nm," *Biomed. Opt. Express*, vol. 9, no. 5, pp. 2326–2335, 2018.

[17] T. Wu *et al.*, "Miniaturized precalibration-based lissajous scanning fiber probe for high speed endoscopic optical coherence tomography," *Opt. Lett.*, vol. 45, no. 8, pp. 2470–2473, Apr. 2020.

[18] K. H. Kim *et al.*, "Two-axis magnetically-driven MEMS scanning catheter for endoscopic high-speed optical coherence tomography," *Opt. Express*, vol. 15, no. 26, pp. 18130–18140, Dec. 2007.

[19] J. Yao *et al.*, "A single-fiber endoscope scanner probe utilizing two-degrees-of-freedom (2DOF) high-order resonance to realize larger scanning angle," *IEEE Trans. Compon., Packag., Manuf. Technol.*, vol. 9, no. 12, pp. 2332–2340, Dec. 2019.

[20] Y.-H. Seo, K. Hwang, H.-C. Park, and K.-H. Jeong, "Electrothermal MEMS fiber scanner with Lissajous patterns for endomicroscopic applications," *Opt. Express*, vol. 24, no. 4, pp. 3903–3909, 2016.

[21] Y.-H. Seo, K. Hwang, and K.-H. Jeong, "1.65 mm diameter forward-viewing confocal endomicroscopic catheter using a flip-chip bonded electrothermal MEMS fiber scanner," *Opt. Express*, vol. 26, no. 4, pp. 4780–4785, 2018.

[22] Q. A. A. Tanguy *et al.*, "Real-time Lissajous imaging with a low-voltage 2-axis MEMS scanner based on electrothermal actuation," *Opt. Express*, vol. 28, no. 6, pp. 8512–8527, Mar. 2020.

[23] J. Sun *et al.*, "3D *in vivo* optical coherence tomography based on a low-voltage, large-scan-range 2D MEMS mirror," *Opt. Express*, vol. 18, no. 12, pp. 12065–12075, Jun. 2010.

[24] C. Duan, Q. Tanguy, A. Pozzi, and H. Xie, "Optical coherence tomography endoscopic probe based on a tilted MEMS mirror," *Biomed. Opt. Express*, vol. 7, no. 9, pp. 3345–3354, Sep. 2016.

[25] H. Li, K. R. Oldham, and T. D. Wang, "3 degree-of-freedom resonant scanner with full-circumferential range and large out-of-plane displacement," *Opt. Express*, vol. 27, no. 11, pp. 16296–16307, May 2019.

[26] T. Kobayashi, T. Matsunaga, and Y. Haga, "Active bending electric endoscope using shape memory alloy wires," in *New Trends in Medical and Service Robots* (Mechanisms and Machine Science), vol. 38, H. Bleuler, M. Bouri, F. Mondada, D. Pisla, A. Rodic, and P. Helmer, Eds. Cham, Switzerland: Springer, 2016, pp. 131–139.

[27] S. Yang and Q. Xu, "A review on actuation and sensing techniques for MEMS-based microgrippers," *J. Micro-Bio Robot.*, vol. 13, nos. 1–4, pp. 1–14, Oct. 2017.

[28] A. A. Ahrabi, M. Kaur, Y. Li, P. Lane, and C. Menon, "An electrothermal actuation method for resonance vibration of a miniaturized optical-fiber scanner for future scanning fiber endoscope design," *Actuators*, vol. 8, no. 1, p. 21, 2019.

[29] P. K. Sarkar *et al.*, "DNA-based fiber optic sensor for direct *in-vivo* measurement of oxidative stress," *Sens. Actuators B, Chem.*, vol. 255, pp. 2194–2202, Feb. 2018.

[30] M. Tao, Y. Jin, N. Gu, and L. Huang, "A method to control the fabrication of etched optical fiber probes with nanometric tips," *J. Opt.*, vol. 12, no. 1, Jan. 2010, Art. no. 015503.

[31] P. Lambelet, A. Sayah, M. Pfeffer, C. Philipona, and F. Marquis-Weible, "Chemically etched fiber tips for near-field optical microscopy: A process for smoother tips," *Appl. Opt.*, vol. 37, no. 31, pp. 7289–7292, Nov. 1998.

[32] A. Foti *et al.*, "A shape-engineered surface-enhanced Raman scattering optical fiber sensor working from the visible to the near-infrared," *Plasmonics*, vol. 8, no. 1, pp. 13–23, Mar. 2013.

[33] D. J. Inman, "Distributed-parameter systems," in *Engineering Vibrations*, 4th ed. New Jersey, NJ, USA: Pearson, vol. 2014, pp. 532–540.

[34] E. C. Haight and W. W. King, "Stability of nonlinear oscillations of an elastic rod," *J. Acoust. Soc. Amer.*, vol. 52, no. 3B, pp. 899–911, Sep. 1972.

[35] M. W. Hyer, "Whirling of a base-excited cantilever beam," *J. Acoust. Soc. Amer.*, vol. 65, no. 4, pp. 931–939, 1979.

[36] L. Wu, Z. Ding, and G. Huang, "Realization of 2D scanning pattern of a fiber cantilever by nonlinear coupling," *Proc. SPIE*, vol. 6534, pp. 653401-1–653401-8, 2006.

[37] OmniVision. (Mar. 2020). *OVM6948*. OmniVision. Accessed: Mar. 28, 2020. [Online]. Available: https://www.ovt.com/sensors/OVM6948

[38] Y.-H. Seo, K. Hwang, H.-C. Park, and K.-H. Jeong, "Electrothermal MEMS fiber scanner for optical endomicroscopy," *Opt. Express*, vol. 24, no. 4, pp. 3903–3909, Feb. 2016.

[39] H.-C. Park, Y.-H. Seo, and K.-H. Jeong, "Lissajous fiber scanning for forward viewing optical endomicroscopy using asymmetric stiffness modulation," *Opt. Express*, vol. 22, no. 5, pp. 5818–5825, 2014.

[40] C. J. Engelbrecht, R. S. Johnston, E. J. Seibel, and F. Helmchen, "Ultra-compact fiber-optic two-photon microscope for functional fluorescence imaging *in vivo*," *Opt. Express*, vol. 16, no. 8, pp. 5556–5564, Apr. 2008.

[41] C. M. Lee, J. E. Chandler, and E. J. Seibel, "Wide field fluorescence imaging in narrow passageways using scanning fiber endoscope technology," *Proc. SPIE*, vol. 7558, Feb. 2010, Art. no. 755806.

Mandeep Kaur received the bachelor's and master's degrees in mechanical engineering from the University of Cassino, Italy. She is currently pursuing the Ph.D. degree in engineering science with the Simon Fraser University.

She is currently working on the design of a sub-millimeter sized catheter. Her research interest includes the fabrication of medical devices for the early detection of cancer.

Malcolm Brown is currently pursuing the bachelor's degree with the Department of Engineering Science, Simon Fraser University, Canada. His research started at SFU's Menrva Research Group, writing data acquisition and display software. He then worked at the BCCRC, where he focused on reconstructing images in real time from captured light.

Pierre M. Lane (Member, IEEE) received the B.Eng. Mgt. in engineering physics from McMaster University, the M.A.Sc. degree in electrical engineering from the Technical University of Nova Scotia, and the Ph.D. degree in electrical and computer engineering from Dalhousie University.

He is currently a Senior Scientist with the BC Cancer Research Center and a Professor of professional practiced with the School of Engineering Science, Simon Fraser University. His research interests include fluorescence and reflectance imaging for early detection of cancer, optical signal and image processing, fiber optics, biophotonics, confocal microscopy, spectroscopy, optical coherence tomography (OCT), and spatial light modulation. He is a member OSA, SPIE. He is also a Professional Engineer registered in the province of British Columbia.

Carlo Menon (Member, IEEE) received the Laurea degree in mechanical engineering and the Ph.D. degree from the University of Padua, Italy, in 2001 and 2005, respectively.

He was a Research Fellow with the European Space Agency, The Netherlands, in 2005 and 2006. In 2007, he joined Simon Fraser University (SFU), Canada, and founded the Menrva Research Group. He is currently a Professor with the School of Mechatronic Systems and Engineering Science, SFU. He has published over 300 articles including journal articles and conference papers. He received several research and career awards including the International IAF Luigi G. Napolitano Award, the International BIONIS Award, the Career Investigator Award from the Michael Smith Foundation for Health Research (MSFHR), the New Investigator Award from the Canadian Institutes of Health Research (CIHR), and the Tier 1 Canada Research Chair (CRC).